View metadata, citation and similar papers at core.ac.uk
brought to you by CORE
provided by Open Access LMU

Jahn-Teller Stabilization of a "Polar" Metal Oxide Surface: $Fe_3O_4(001)$

R. Pentcheva,[1,*] F. Wendler,[1] H. L. Meyerheim,[1,†] W. Moritz,[1] N. Jedrecy,[2] and M. Scheffler[3]

[1]*Department of Earth and Environmental Sciences, University of Munich, Theresienstrasse 41, 80333 Munich, Germany*
[2]*Laboratoire Mineralogie-Cristallographie, Université Paris 6 et 7, 4 place Jussieu, F-75252 Paris, France*
[3]*Fritz-Haber-Institut der Max-Planck-Gesellschaft, Faradayweg 4-6, D-14195 Berlin, Germany*

(Received 4 June 2004; published 1 April 2005)

Using *ab initio* thermodynamics we compile a phase diagram for the surface of $Fe_3O_4(001)$ as a function of temperature and oxygen pressures. A hitherto ignored polar termination with octahedral iron and oxygen forming a *wavelike* structure along the [110] direction is identified as the lowest energy configuration over a broad range of oxygen gas-phase conditions. This novel geometry is confirmed via x-ray diffraction analysis. The stabilization of the $Fe_3O_4(001)$ surface goes together with dramatic changes in the electronic and magnetic properties, e.g., a half metal to metal transition.

DOI: 10.1103/PhysRevLett.94.126101 PACS numbers: 68.35.Md, 68.35.Bs, 68.47.Gh, 73.20.At

The surface composition and structure of a multicomponent material is a fundamental property that has significant consequences for its surface reactivity, mechanical, and magnetic properties. Magnetite is not only important in geophysics and mineralogy, but is also attracting increasing attention as a potential material for spintronic devices [1,2], due to the predicted half-metallic behavior [3], coupled with a high Curie temperature of 858 K.

Magnetite crystallizes in the inverse spinel structure, where the oxygen atoms form a slightly distorted face centered cubic lattice and the iron atoms occupy tetrahedral and octahedral interstitial sites. The stacking sequence in the [001] direction consists of A layers containing tetrahedral iron (Fe_A) and B layers with oxygen and octahedral iron (Fe_B) atoms (cf. Fig. 1).

Two alternative approaches are widely used to assess possible terminations for metal oxide surfaces: an ionic scheme considering the electrostatic energy [4] and the autocompensation rule applied to covalent bonds [5]. After the scheme of Tasker [4], bulk truncations of the $Fe_3O_4(001)$ surface should be unstable because of a diverging surface energy due to uncompensated dipole moments. Such structures were, therefore, so far discarded. Both the ionic [4] and the covalent [5] approach rely on the information from the bulk only and suggest that stabilization of a polar surface can be achieved only through massive changes of the surface stoichiometry.

For $Fe_3O_4(001)$ a $(\sqrt{2}\times\sqrt{2})R45°$ reconstruction has been observed experimentally [6–11]. However, the surface structure and stoichiometry are still under debate. Applying the autocompensation rule [5] to $Fe_3O_4(001)$, two models for the $(\sqrt{2}\times\sqrt{2})R45°$ reconstruction have been proposed so far: an A layer where half of the tetrahedral iron is missing [7–9] and a B layer with oxygen vacancies or hydroxyl groups [10,11]. Several variations of the former model have been suggested: The x-ray photoelectron diffraction analysis of Chambers *et al.* [8] and the low energy ion scattering results of Mijiritskii *et al.* [9] were interpreted as a half-filled A layer with strong inward relaxations of the surface layers. Concerning the magnitude of the interlayer distances, there is a considerable discrepancy. In a molecular dynamics calculation with classical potentials (the only theoretical work so far) Rustad *et al.* [12] suggested a 0.5 monolayer (ML) A termination where the surface and half of the subsurface Fe_A relax in octahedral positions in the surface B layer. Also nonautocompensated terminations with a charge ordered B layer were reported from scanning tunneling microscopy (STM) measurements using a ferromagnetic [13] or an antiferromagnetic tip [14]. However, the observed magnetic contrast alone cannot explain the LEED and x-ray diffraction (XRD) superstructure intensities and does not provide a clue to the stabilization mechanism of the surface.

In this Letter we present the results of a systematic investigation of the composition, structure, and properties of the $Fe_3O_4(001)$ surface based on density-functional theory (DFT) calculations. Using *ab initio atomistic thermodynamics* [15,16], we predict that a "polar" termination is the lowest energy configuration over the entire range of accessible oxygen pressures. The stabilization of the surface involves a fundamentally different mechanism, which has not been considered so far: While most of the previous

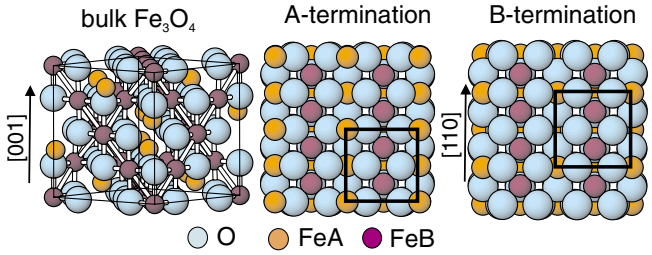

FIG. 1 (color online). The inverse spinel structure of magnetite together with a top view of the two bulk truncations of $Fe_3O_4(001)$ with an A and a B layer, respectively. Oxygen atoms, Fe_B, and Fe_A are marked by white (light blue), gray (orange), and black (purple) circles.

 © 2005 The American Physical Society

studies proposed an ordering of surface vacancies as the origin of the surface reconstruction, here it is explained as a Jahn-Teller distortion of the surface atoms forming a *wave-like* pattern along the [110] direction. An XRD analysis supports this theoretically predicted model.

We use the full-potential augmented plane wave (FP-APW) method in the WIEN2k implementation [17] and the generalized gradient approximation (GGA) [18]. The $Fe_3O_4(001)$ surface is modeled by a symmetric slab containing five B and four to six A layers depending on the structural model. The vacuum between the repeated slabs amounts to 10 Å. We have ensured convergence with respect to the thickness of the slab by repeating the calculations for the most stable configurations with a thicker slab with an additional A and a B layer on both sides (approximately 100 atoms in the unit cell as opposed to 70 in the original unit cell). The surface free energies for both supercells are within ± 3 meV/Å^2 equal. The lateral parameter of the supercell is set to the GGA bulk lattice constant, 8.42 Å, which is in good agreement with the experimental value of 8.394 Å.

A mixed APW + lo (local orbitals) and linearized augmented plane waves basis set was used with $R_{\mathrm{Fe}}^{\mathrm{MT}} = 1.90$ bohr, $R_{\mathrm{O}}^{\mathrm{MT}} = 1.40$ bohr. Inside the muffin tins (MTs) wave functions are expanded in spherical harmonics up to $l_{\mathrm{max}}^{\mathrm{wf}} = 10$, and nonspherical contributions to the electron density and potential are considered up to $l_{\mathrm{max}}^{\mathrm{pot}} = 4$. The energy cutoff for the plane wave representation in the interstitial is $E_{\mathrm{max}}^{\mathrm{wf}} = 19$ Ry for the wave functions and $E_{\mathrm{max}}^{\mathrm{pot}} = 196$ Ry for the potential. With these cutoff parameters an accuracy of energy differences better than 1 mRy is achieved. Results for the $(\sqrt{2} \times \sqrt{2})R45°$ unit cell are obtained with $4k_{\parallel}$ points in the irreducible part of the Brillouin zone.

The configurations we have considered include 0.5 ML of tetrahedral iron (i) above the B layer [7–9] or (ii) relaxed in the B layer, and (iii) a modified 0.5 ML A termination where the surface and half of the subsurface Fe_A occupies octahedral sites in the B layer [12]. Additionally, we have considered two geometries with one oxygen vacancy per unit cell: either as a nearest neighbor to a tetrahedral iron or above an octahedral iron. Together with the nonautocompensated A and B terminations shown in Fig. 1 they were used as a starting point for the DFT calculations, where we performed a full structural optimization of the atomic positions in the outer two AB double layers with damped Newton dynamics [19].

The calculated surface phase diagram for all studied terminations is compiled in Fig. 2. The oxygen chemical potential is converted into oxygen pressures for a fixed temperature of $T = 900$ K, which corresponds to a typical annealing temperature in experiment. The range of allowed oxygen chemical potentials lies between the ''oxygen-poor'' limit, which corresponds to the case where the oxide would decompose in iron crystallites and oxygen gas, and the ''oxygen-rich'' limit, defined by the chemical potential of oxygen in the oxygen molecule, set as zero reference. In Fig. 2 the surface energy is given with respect to bulk magnetite. We note that at $T = 900$ K and $p'_{\mathrm{O}_2} > 10^{-6}$ mbar hematite becomes the thermodynamically stable phase [20]. Taking into account the calculated enthalpy of formation for magnetite (11.32 eV) and hematite (8.024 eV) [21], the stability range of Fe_3O_4 extends up to $\mu_{\mathrm{O}} = -1.5$ eV.

Autocompensated terminations, e.g., the ones containing 0.5 ML Fe_A in the surface layer, are independent of the oxygen pressure, while the effect of the oxygen environment is most distinct for the two bulk truncations with an A or a B layer. In line with electrostatic considerations, the A termination is unstable, and this trend is substantially enhanced for *oxygen-rich* conditions. A most striking result is that the other bulk truncated surface, the B termination, which has been so far discarded as a noncompensated

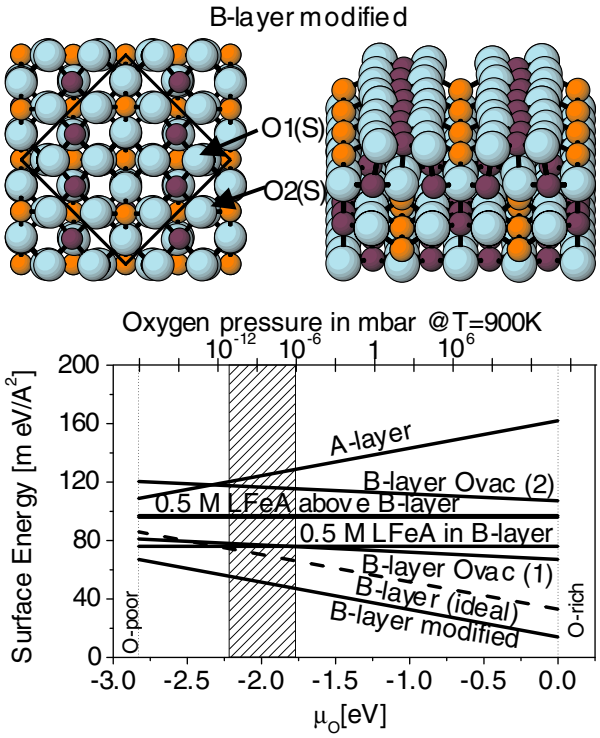

FIG. 2 (color online). Calculated surface free energy $\gamma(T, p)$ as a function of the chemical potential of oxygen (bottom x axis) for all studied terminations. In the top x axis μ_{O} is converted into a pressure scale at $T = 900$ K. The vertical lines mark the oxygen-poor and oxygen-rich limits of the oxygen chemical potential, with $1/2E_{\mathrm{O}_2}^{\mathrm{total}}$ used as zero reference. The dashed region marks the range of pressures that were used during sample preparation in the experiment. The B termination with bulk atomic positions and modified positions with a $(\sqrt{2} \times \sqrt{2})R45°$ periodicity are marked as ideal and modified, respectively. The B layer with oxygen vacancies above an octahedral iron and next to a tetrahedral iron are denoted by (1) and (2), respectively. Top and side views of the modified B layer are given at the top. Surface oxygens with and without a Fe_A neighbor are denoted by O2(S) and O1(S), respectively. For the color code see Fig. 1.

surface, turns out to be the most stable configuration over a broad range of oxygen pressures even in the ideal (unrelaxed) geometry. For oxygen-poor conditions it competes with a 0.5 ML tetrahedral Fe relaxed in the B layer and with a B termination with O vacancies lying above an octahedral iron in the subsurface B layer.

An asymmetric force on the surface oxygens in the unreconstructed ideal B termination entails a wavelike distortion along the Fe_B row. Hence, the origin of the symmetry reduction and the observed $(\sqrt{2} \times \sqrt{2})R45°$ pattern is a Jahn-Teller distortion [22,23]. Compared to the ideal B termination, the formation of this *modified B* termination is connected with an energy gain of approximately 20 meV/Å^2 and a reduction of the work function of 0.46 eV from 5.78 to 5.32 eV. We note that a reduction of Φ indicates a decrease of the dipole moment induced on the surface, i.e., a decrease in polarity. The calculated work function is in good agreement with the value measured in photoemission experiments [24].

A top and a side view of the novel surface geometry are given in Fig. 2 (top). The wavelike pattern along the [110] direction emerges from a strong lateral relaxation of 0.30 Å of one of the two oxygen atoms with a missing Fe_A neighbor [marked as O1(S) in Fig. 2] towards the Fe_B row and a subsequent alternating shift of Fe_B pairs by ± 0.09 Å perpendicular to the Fe_B row. The oxygen atoms with a Fe_A neighbor [O2(S)] relax by 0.14 Å towards and by 0.03 Å parallel to the Fe_B row. Because of the lateral relaxation of oxygen, the Fe_B oxygen distance is reduced from 2.06 Å in the bulk to 1.96 Å on the surface and is thus closer to the bulk values for the tetrahedral ($d^{\text{bulk}}_{\text{O-Fe}_A} = 1.89$ Å) coordination. Perpendicular to the surface, all surface atoms relax inwards except for O1(S), which relaxes outwards. The atoms in the subsurface A and B layers relax outwards. A detailed structural analysis will be presented elsewhere [25].

X-ray measurements were performed on a natural crystal [26] at the beam line DW12 at LURE, Orsay, with a wavelength of 0.826 Å. In total, 220 symmetrically independent reflections were measured at room temperature in five crystal truncation rods and six superstructure rods. The cleanliness of the sample and the reproducibility of the $(\sqrt{2} \times \sqrt{2})R45°$ LEED pattern were verified by a repeated sputtering and annealing of the sample up to 850 K in UHV and oxygen pressures up to 5×10^{-6} mbar. Furthermore, the LEED I/V curves of the natural and an artificial crystal are nearly identical [27].

To minimize the effect of surface inhomogeneities, only the superstructure reflections were considered in the analysis. The experimental data and the calculated curves for the two most promising terminations, i.e., the half-filled A layer of tetrahedral iron and the modified B termination, are displayed in Fig. 3. The corresponding R factors obtained after a structural refinement with the DFT geometries are 0.24 and 0.19, respectively, which indicates a preference for the modified B termination. Both models vary only by the additional tetrahedral iron in the half-filled A layer. The relaxations of the remaining atoms are rather similar, leading to an overall similarity in the intensity distribution along q_z. Still the fit with the modified B layer is noticeably better. The B termination with oxygen vacancies, proposed by Stanka *et al.* [10], is incompatible with the XRD data (R factor worse than 0.6). The wavelike structure along the [110] direction observed in the STM measurements of Stanka *et al.* [10] is rather a further evidence for the modified B termination [28].

The stabilization of the $Fe_3O_4(001)$ surface and the unusual lattice distortions are connected with strong changes in the electronic and magnetic properties. In the bulk, magnetite shows a *half-metallic* behavior with a band gap in the majority spin channel of approximately 0.5 eV and a 100% spin polarization due to the t_{2g} states of Fe_B at E_F in the minority spin channel [3].

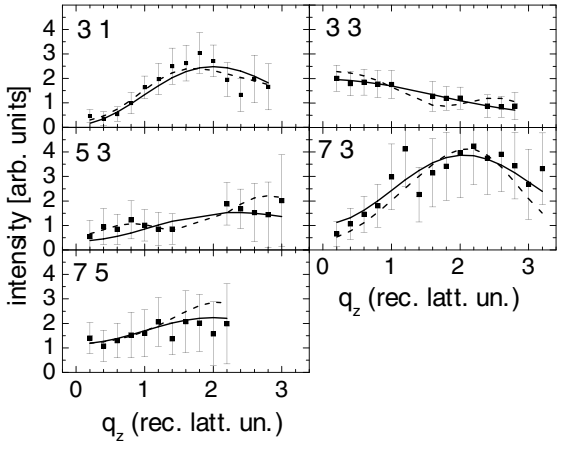

FIG. 3. Results of the XRD analysis. The experimental data are marked by squares. Solid and dashed lines correspond to fits assuming the modified B termination and 0.5 ML Fe_A termination, respectively.

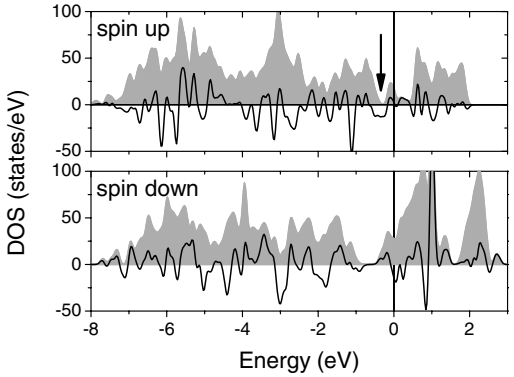

FIG. 4. Total density of states (DOS) of $Fe_3O_4(001)$ terminated by a modified B layer for the majority (minority) spin channel in the upper (lower) panel is shown in gray. The difference of the DOS of the modified B termination and the bulk-terminated B layer is given with a black line. A Gauss broadening of $2\sigma = 0.05$ eV is used.

The surface states in the majority spin gap (cf. Fig. 4) reduce the spin polarization at the Fermi level to approximately 40%. Spin-resolved photoemission measurements support this result [24]. Since electrons near the Fermi level are important for transport properties, we examined their nature more closely: the states at E_F are confined to the surface layer and are due to the hybridization between $d_{x_2-y_2}$ states of Fe_B and p_x, p_y states of O1(S). Additionally, there is a noticeable contribution from the tetrahedral iron in the subsurface layer. To get more insight into the driving mechanisms towards the reconstruction of the surface, we plotted in Fig. 4 also the difference between the density of states (DOS) of the B termination with modified and ideal positions of the atoms. For the modified B termination a band gap opens in the majority spin channel between -0.4 and -0.2 eV where states of $d_{x_2-y_2}(d_{z_2})$ character are shifted to higher (lower) energies. The latter cross the Fermi level and eventually become partially unoccupied. Vice versa, in the minority spin channel, bands become occupied. Altogether this reduces the energy of the system.

This combination of a Jahn-Teller distortion and a spin flip leads to interesting magnetic properties. In the bulk magnetite is a ferrimagnet with the magnetic moments of tetrahedral ($-3.43\mu_B$) and octahedral iron ($3.50\mu_B$) oriented antiparallel to each other and a total magnetic moment of $4.0\mu_B$ per formula unit. In the modified B termination the magnetic moments of the subsurface Fe_A ($-3.45\mu_B$) is close to the bulk value. However, the magnetic moment of the surface Fe_B ($3.00\mu_B$) is substantially reduced due to the strong relaxations.

Additionally, a substantial magnetic moment of approximately $0.25\mu_B$ is induced in the undercoordinated surface oxygen with a missing bond to tetrahedral iron, while the magnetic moments of the rest of the surface oxygen atoms are close to the bulk value, $0.07\mu_B$. A similar magnetization was observed for the oxygen-terminated $\alpha-Fe_2O_3(0001)$ surface [21].

Based on *ab initio* thermodynamics we identify a B termination with octahedral iron and oxygen in the surface layer forming a wavelike structure along the [110] direction as the thermodynamically stable configuration over a broad range of oxygen pressures. Instead of an ordering of surface defects the symmetry reduction is achieved by a Jahn-Teller distortion and is connected with strong changes of the electronic and magnetic properties, e.g., a metallization at the surface. Experimental evidence for the DFT-predicted geometry is given in STM measurements [10,24] and an XRD analysis performed with the atomic positions obtained with DFT.

Theoretically, polar surfaces have been predicted for a number of metal oxide surfaces, e.g., $Fe_2O_3(0001)$ [21], $RuO_2(110)$ [16], ZnO(0001) [29], and PdO [30]. The modified B termination of $Fe_3O_4(001)$ is a further example that excluding such surfaces from the structural analysis can be misleading.

This work was supported by the DFG, PE 883.

*Electronic address: pentcheva@lrz.uni-muenchen.de
†Permanent address: MPI für Mikrostrukturphysik, Weinberg 2, 06120 Halle, Germany.

[1] M. A. M. Gijs and P. J. Kelly, European Patent No. EP 0 672 303 A1 (1995).
[2] W. Eerenstein *et al.*, Phys. Rev. Lett. **88**, 247204 (2002).
[3] Z. Zhang and S. Satpathy, Phys. Rev. B **44**, 13 319 (1991).
[4] P. W. Tasker, J. Phys. C **12**, 4977 (1979).
[5] J. P. LaFemina, Crit. Rev. Surf. Chem. **3**, 297 (1994).
[6] J. M. Gaines *et al.*, Surf. Sci. **373**, 85 (1997).
[7] G. Tarrach *et al.*, Surf. Sci. **285**, 1 (1993).
[8] S. A. Chambers, S. Thevuthasan, and S. A. Joyce, Surf. Sci. **450**, L273 (2000).
[9] A. V. Mijiritskii and D. O. Boerma, Surf. Sci. **486**, 73 (2001).
[10] B. Stanka *et al.*, Surf. Sci. **448**, 49 (2000).
[11] F. C. Voogt *et al.*, Phys. Rev. B **60**, 11 193 (1999).
[12] J. R. Rustad, E. Wasserman, and A. R. Felmy, Surf. Sci. **432**, L583 (1999).
[13] R. Wiesendanger *et al.*, Science **255**, 583 (1992).
[14] G. Mariotto, S. Murphy, and I. V. Shvets, Phys. Rev. B **66**, 245426 (2002).
[15] C. M. Weinert and M. Scheffler, in *Defects in Semiconductors*, edited by H. J. Bardeleben, Materials Science Forum Vols. 10–12 (Trans Tech Publications, Ltd., Aedermannsdorf, Switzerland, 1986), p. 25.
[16] K. Reuter and M. Scheffler, Phys. Rev. B **65**, 035406 (2002).
[17] P. Blaha, K. Schwarz, G. K. H. Madsen, D. Kvasnicka, and J. Luitz, *WIEN2k, An Augmented Plane Wave + Local Orbitals Program for Calculating Crystal Properties*, edited by Karlheinz Schwarz (Technical University of Wien, Austria, 2001), ISBN 3-9501031-1-2.
[18] J. P. Perdew, K. Burke, and M. Ernzerhof, Phys. Rev. Lett. **77**, 3865 (1996).
[19] B. Kohler *et al.*, Comput. Phys. Commun. **94**, 31 (1996).
[20] F. D. Richardson and J. H. E. Jeffes, J. Iron Steel Industry **160**, 261 (1948).
[21] X.-G. Wang *et al.*, Phys. Rev. Lett. **81**, 1038 (1998).
[22] H. A. Jahn and E. Teller, Proc. R. Soc. London A **161**, 220 (1937).
[23] The total energy as a function of the distortion shows a cusp at the symmetric initial configuration and is thus in accord with the Jahn-Teller theorem.
[24] M. Fonin *et al.* (private communication).
[25] R. Pentcheva *et al.* (to be published).
[26] Besides 0.02% Mn no contaminations of the crystal were detected with x-ray fluorescence spectroscopy.
[27] S. Frank, D. Schrupp, and W. Moritz (private communication).
[28] STM simulations performed in the Tersoff-Hamann model are consistent with the STM images of Stanka *et al.* [10]. These results will be published elsewhere.
[29] O. Dulub, U. Diebold, and G. Kresse, Phys. Rev. Lett. **90**, 016102 (2003).
[30] J. Rogal, K. Reuter, and M. Scheffler, Phys. Rev. B **69**, 075421 (2004).